A comparison study on fin surfaces in finned-tube heat exchangers

Tony W.H. Sheu and S.F Tsai
Department of Naval Architecture and Ocean Engineering, National Taiwan University, Taipei, Taiwan, R.O.C.

Received April 1997
Revised October 1997
Accepted December 1997

Keywords *Fins, Heat exchanger, Surfaces*

Abstract *A three-dimensional numerical study was conducted to assess the heat transfer performance of extended fins in a two-row finned tube heat exchanger. Fins under investigation were plane and slit types. A finite volume discretization method and a SIMPLE-based solution algorithm were, respectively, applied to working differential equations and their discrete counterparts to compute the gas velocities and pressure. The temperatures of solid and gas phases were computed from the same energy equation with different diffusivities and prescribed convective fluxes. The main objective of this study was to compare the transfer capabilities of the two investigated fin shapes. Their capabilities as a whole are presented in terms of the computed Nusselt number and the pressure drop across the flow passage.*

Introduction

Finned tube heat exchangers have been used for heat transfer between gas and solid phases for many years. Given that the density and thermal conductivity of gases are both much lower than those of liquids, heat transfer is poor. To alleviate this deterioration in heat transfer capabilities when gas is used as the working medium, it is important to add an *ad hoc* secondary fin surface to enhance heat transfer without losing the compactness of the conjugate heat exchangers. Besides the extended fin surface, the tube arrangement plays a crucial role in determining the capability of the finned tube heat exchanger. According to Saboya and Sparrow (1974; 1976), a staggered tube arrangement provides higher performance compared to an in-line tube arrangement. The present analysis is, thus, concentrated on air flow through two-row staggered tubes. Owing to space considerations, the tubes under investigation are those with fixed values of the dimensionless length ratios. No attempt will be made to justify whether tubes arranged in a two-row staggered configuration, positioned with equilateral triangular centers, are superior to other combinations.

The flow pattern observed in the plate and tube heat exchanger configuration can be very complex due to the three-dimensional helical horseshoe vortices and flow separations. Analyses can be further

International Journal of Numerical Methods for Heat & Fluid Flow, Vol. 9 No. 1, 1999, pp. 92-106,

The authors would like to thank Fred E.C. Huang, H.H. Lin, J. Chien, J.Y. Lee, Y.C. Lin, J.H. Wu, W.M. Hu and C.P. Chiang of the Teco Electric and Machinery Co. Ltd who provided experimental data and useful information in the course of this study.

complicated by the added complexities of extended surfaces. In the past decade, little progress has been made in measuring the local heat transfer coefficient because "no experimental method exists that allows measurement of the conjugate local heat transfer of a finned-tube element" (Fiebig *et al.*, 1995a; b). With the advent of highspeed computers and ever-improving numerical analyses, it is now possible to numerically predict the heat transfer characteristics in a three-dimensional context. In this study, we exploited the computational fluid dynamics technique to assess the transfer capabilities of two classes of fin surfaces. Their capabilities, as a whole, can be presented in terms of some parameters. The span-averaged Nusselt number and pressure drop are among those parameters addressed in this article.

We begin by introducing the working Navier-Stokes equations for the flow field while using the energy equation for the temperature field. This is followed by a brief description of the underlying finite volume discretization method, the solution algorithm, and the multi-dimensional advection scheme for the nonlinear flux terms. To verify the developed computer code for the two investigated fin-tube heat exchanger configurations, validation against analytic data is presented. Prior to discussing in detail the complex flow structure, we describe the investigated conjugate heat transfer problem. In the Results section, attention is given to the interaction structure of the horseshoe vortex and the wake behind the tube. Plausible reasons for the formation of helical vortices are also addressed. We end with closing remarks.

Theoretical analysis

Mathematical model

Since the Mach number of air in the passage of daily-used forced convection heat exchangers is much smaller than 0.2, analysis can be rationally conducted within the incompressible framework. To numerically explore the heat transfer characteristics of fins, conventional analyses are carried out by simply solving the fin conduction equation with an assumed distribution of the convective heat transfer coefficient on the fin surface. In practical circumstances, the heat transfer coefficient varies to a great extent along the fin surface. Approaches which are based on an assumed constant heat transfer coefficient, while facilitating analysis, may lead to uncertain results. This fact provides us with strong motivation for developing a mathematical model for simultaneous solution of the conduction equation for the fin itself and the convective equation for a gaseous fluid. In the absence of gravity, a complete set of conservation equations for the flow field is given by the following elliptic-parabolic type of partial differential equations for a given Reynolds number defined in Table I:

$$\frac{\partial u_i}{\partial x_i} = 0, \qquad \text{in } \Omega, \tag{1}$$

$$Re = \frac{\dot{m} D_h}{A_c \nu} = \frac{U D_h}{\nu} \frac{A}{A_c}$$

$\dot{m}$ = flow rate of air
D_h = hydraulic diameter
= $(4A_c L)/(A_f + \pi DH/4)$
A_c = minimum flow area in a unit cell
A_f = transfer area for a unit cell
D = tube diameter
L = streamwise length of the channel
H = spacing between plates
A = maximum flow area of a unit cell
U = inlet velocity

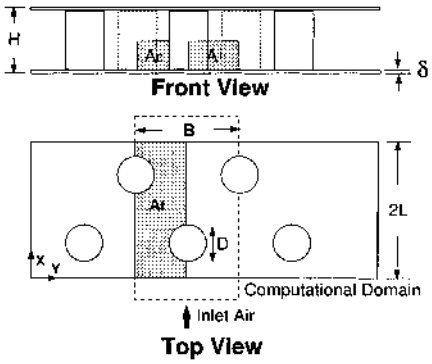

case	inlet velocity U (m/s)	Reynolds number
1	0.81	83
2*	1.00	103
3	1.20	124
4*	1.50	155
5	1.81	186
6	2.00	206
7*	2.50	258

Experimental data are available

Table I.
Definition of Reynolds numbers and running flow conditions

$$\frac{\partial u_i}{\partial t} + \frac{\partial}{\partial x_m}(u_m u_i) = -\frac{\partial p}{\partial x_i} + \frac{1}{Re}\frac{\partial^2 u_i}{\partial x_m \partial x_m} \qquad \text{in } \Omega. \tag{2}$$

The air temperature in the flow passage is computed using the following energy equation which holds in the gas phase:

$$\frac{\partial T}{\partial t} + \frac{\partial}{\partial x_m}(u_m T) = \frac{1}{Pe}\frac{\partial^2 T}{\partial x_m \partial x_m}. \tag{3}$$

The dimensionless parameter Pe in equation (3) denotes the Peclet number which is defined as $Pe = Pr \cdot Re$. Here, Pr is the Prandtl number ($Pr = \frac{\nu}{\alpha}$), which represents the ratio of two diffusivities, namely the fluid viscosity ν and thermal diffusivity α.

In the literature, there exist several sets of working variables to choose from. Of these, the primitive-variable formulation has proven to be the method of choice by many research groups for simulating incompressible fluid flows. The main reason is that this variable setting permits specification of closure boundary and initial conditions (Ladyzhenskaya, 1963). Moreover, these closure conditions are relatively easy to implement in the existing computer code.

It has been known for quite some time that instability is encountered in numerical simulation of equations (1)-(2) using second-order central discretization schemes. This difficulty is particularly severe in situations where advection dominates diffusion. On top of this, the so-called false diffusion error may further cause gross numerical pollution of the flow physics. As a remedy, the third-order QUICK scheme introduced by Leonard (1979) has been widely used to provide stabilization. Recognizing this, the scheme adopted for the present computations is the QUICK scheme, which is formulated in a non-uniform grid system. In arbitrary meshes, errors due to the use of curvilinear coordinate transformation may further obscure the physical phenomena. This is a constant danger, in particular for problems involving stretched and distorted meshes. Therefore, the present analyses were conducted in rectangular grids for better resolution of the flow structure.

We have a choice of simulating equations (1)-(2) in a staggering (Patankar, 1980) or collocating (Abdallah, 1987) grid system. In this study, we abandoned the collocating grid approach in favor of the first strategy. Even at the cost of adding programming complication, the motivation behind seeking solutions in a staggered grid is that the non-staggered approach lacks boundary pressure for analyses involving a Poisson-type of pressure-correction equation. Within the staggered grid context, on the control surface of a finite volume cell, each primitive variable takes over a node to itself whereas the pressure node is surrounded by nodal velocities. This variable setting is suitable when the finite volume integration method is used to discretize each conservation equation under these circumstances.

Solution algorithm

In numerical simulation of incompressible flows, use of a mixed formulation is desirable since it assures satisfaction of the discrete divergence-free constraint condition. This desirable feature is, unfortunately, accompanied by a much larger discrete system to deal with. The need to avoid an excessive computer storage demand has prompted researchers to consider segregated approaches. In the present study, solutions to finite volume discretization equations are obtained sequentially for all the primitive variables. The solutions to equations (1)-(3) are obtained numerically using the SIMPLE iterative solution algorithm. This is quite an involved algorithm which has already been described in Patankar (1980). The concepts and procedures of the underlying algorithm will not be restated here to facilitate a compact presentation. The energy equation (3) is then solved using the computed convergent velocities and the assumed temperatures, which are stored at pressure nodes.

Problem descriptions and boundary conditions

Figures 1 and 2 show the two heat exchanger configurations under investigation. Similarity exists between the target configurations in that there are two rows of cylindrical tubes which are arranged in a staggered array on equilateral

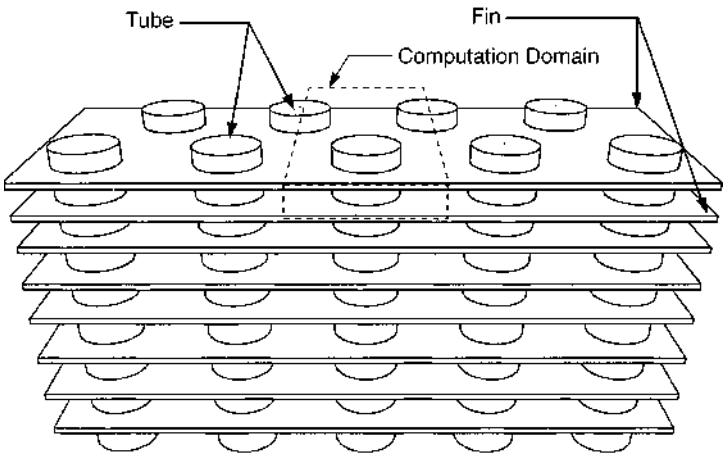

Figure 1.
Schematic of two-row fin and tube heat exchanger configuration. Analysis is conducted in dotted area due to flow periodicity

triangular centers. Close examination of Figure 1 reveals the existence of geometric symmetry, which suggests that the analysis can be conducted in regions bounded within the dashed planes. This finding obviates full-scale computation provided that a periodic boundary condition is prescribed on the dashed-line planes. The computational expense can then be dramatically reduced.

Referring to Figure 3, the fin-tube configuration is with the dimension ratios H/D = 0.187, B/D = 2.72, and L/D = 1.693. Within the computational domain in Figure 3, scaled by $2L$: B: H = 25.5: 20.4: 1.4, the boundary conditions applied at the fin surfaces are $u = v = w = 0$. At the inlet plane which is upstream of the leading edge of the fin with a length of 4.5mm, a uniform free-stream with density ρ = 1.1614kg/m^3, velocity u = 1.2m/s, v = 0 m/s, w = 0m/s, temperature T_∞ = 300K, and kinematic viscosity $\nu = 1.6 \times 10^{-5}$m^2/s approaches the two-row heat exchanger. For the aluminum fin (ρ = 2,707kg/m^3) under investigation, its thickness is 0.115mm, its thermal conductivity k_f = 204W/m·K, and its specific heat at a constant pressure, C_p = 0.896kJ/kg·K. The specific heat of air at the constant pressure is C_p = 1.007kJ/kg·K. In this study, the temperature of the medium inside the cylinder tube remained fixed at 323K. Owing to space considerations, we will restrict our attention to a Reynolds number, as defined by $Re = \frac{UD_h}{\nu}\frac{A}{A_c}$, having a fixed value of 124. It is noted that the Reynolds number and the spacing between two adjacent fins are commonly encountered in the present-day air-conditioning machines.

To save the disk space, it is advantageous to limit the analysis domain to a length which is sufficiently away from the trailing edge of the fin plate. For physical reasons, zero streamwise gradients are prescribed at the synthetic outlet:

$$\frac{\partial u}{\partial x} = \frac{\partial p}{\partial x} = \frac{\partial T}{\partial x} = 0 \,. \tag{4}$$

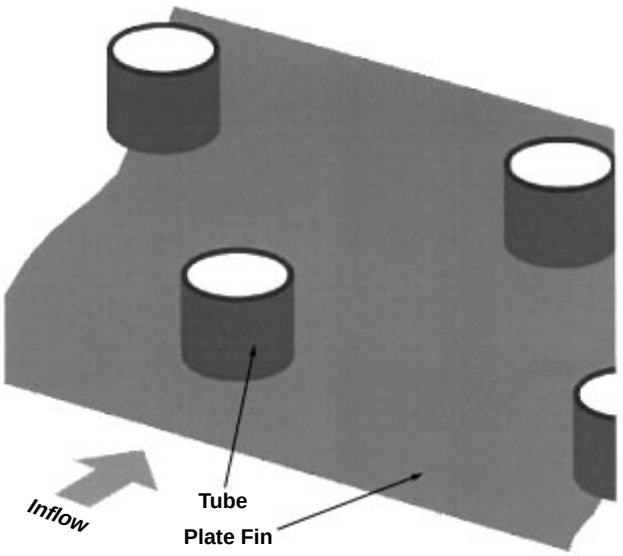

(a)

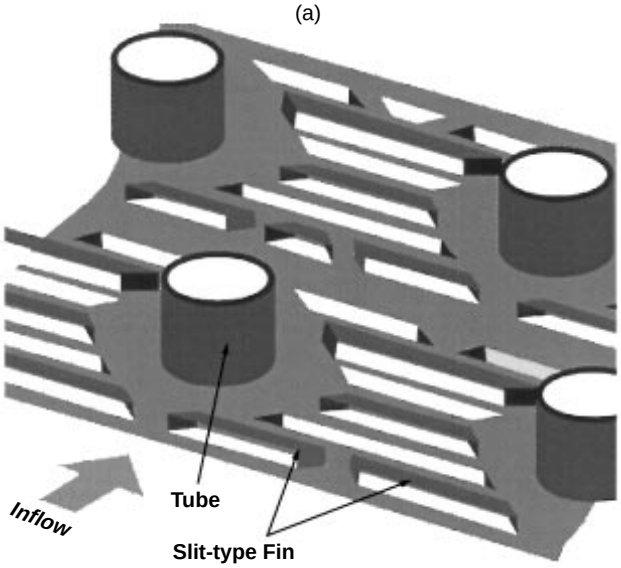

(b)

Figure 2.
Three-dimensional plot of finned-tube surfaces. (a) plate fin surface; (b) slit type extended fin surfaces

To close the differential system, periodic conditions for the velocity vector $\underline{u}$ and the temperature T are prescribed on the rest of the boundary surfaces:

$$\underline{u}(x,0,z) = \underline{u}(x,B,z)\,, \quad \underline{u}(x,y,0) = \underline{u}(x,y,H)\,;$$

$$T(x,0,z) = T(x,B,z)\,, \quad T(x,y,0) = T(x,y,H)\,. \tag{5}$$

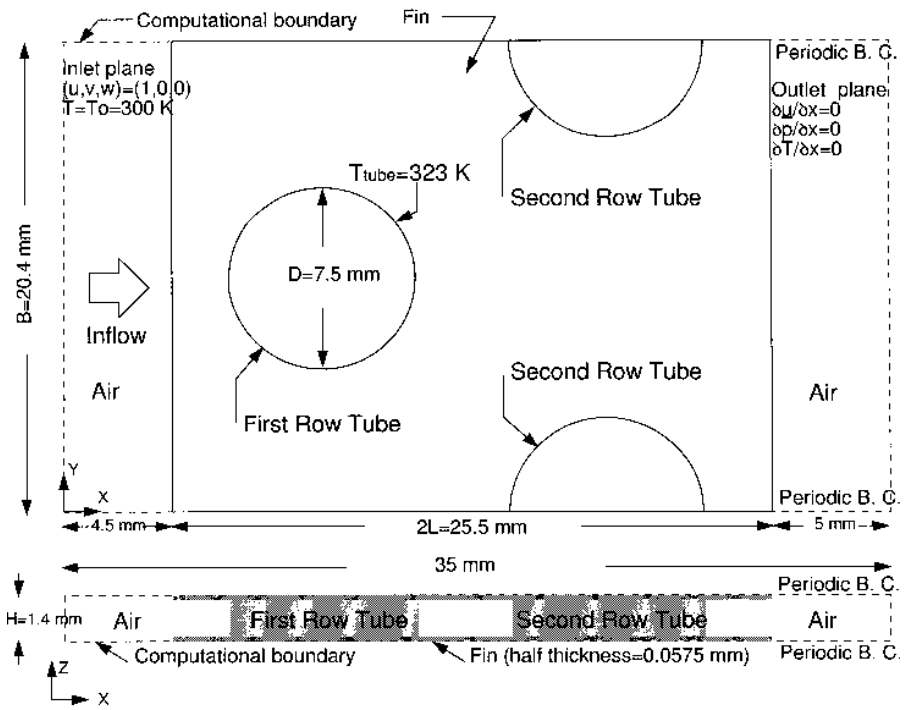

Figure 3.
A finned-tube element as module geometry for the investigation. Included in this figure are also prescribed boundary conditions

Recall that velocity and thermal boundary layers may develop over the no-slip walls, and that grids must be well stretched to capture the high-gradient solution profiles. In this study, the channel is covered with non-uniform grids with a resolution of $142 \times 84 \times 54$.

Results and discussions

Numerical results have been obtained for air with Pr = 0.7 and inlet velocity u = 1.2 m/s. By definition, as given in Table I, the Reynolds number under investigation falls into the range found in commonly encountered finned-tube heat exchangers.

Validation studies

Prior to obtaining the flow physics from the computed finite volume solutions, it is instructive to confirm the applicability of the computer code developed here to simulate heat transfer in a finned-tube heat exchanger. To this end, there are two tasks to be performed. In the first place, a validation study was conducted by considering Navier-Stokes equations which were amenable to analytic solutions. Prediction errors rendered from cases with different mesh sizes were cast in different norms. With these norms, we were able to estimate the rate of convergence for the vector quantities, i.e. the velocities, and scalar quantity, i.e. the pressure p. Owing to space considerations, the analytic study of the

computer code employed here is given elsewhere. Interested readers are referred to Sheu and Lee (1996) for additional details.

The validation study then proceeded to a comparison of the experimental and numerical data. In this study, the pressure drop and the heat transfer rate through the channel passage were chosen for comparison. As Figures 4 and 5 show, the agreement between the measured data of Teco company of Republic of China (private communication) and computed data was acceptable. With the given success in conducting analytic and experimental validations, we had sufficient confidence to explore the physics of the air flow in the finned-tube passage of the heat exchangers using the data so far obtained.

Heat transfer characteristics of the fin surface

To give readers an idea of how effectively different kinds of heat exchangers can transfer heat through an air flow, we plot first the heat flux distribution on fin surfaces for plate as well as for slit type heat exchangers. Figure 6 shows the heat flux $\dot{q}$ on the plate fin for Re = 124. The results show that the largest value of $\dot{q}$ appears in regions adjacent to the leading edge of the finned plate. The reasons for this local maximum value of $\dot{q}$ are twofold. The first one is the developing flow, as seen in Figure 7, over the finned-plate. This flow development yields good convective heat transfer at the leading edge. The reasons for the high value of $\dot{q}$ in regions just upstream of the two tubes are different from those discussed previously in regions near the leading edge. The higher value of $\dot{q}$ observed in the upstream side of the tube is due mainly to the effective mixing between the bulk fluids and fluids either in the neighbor of fin

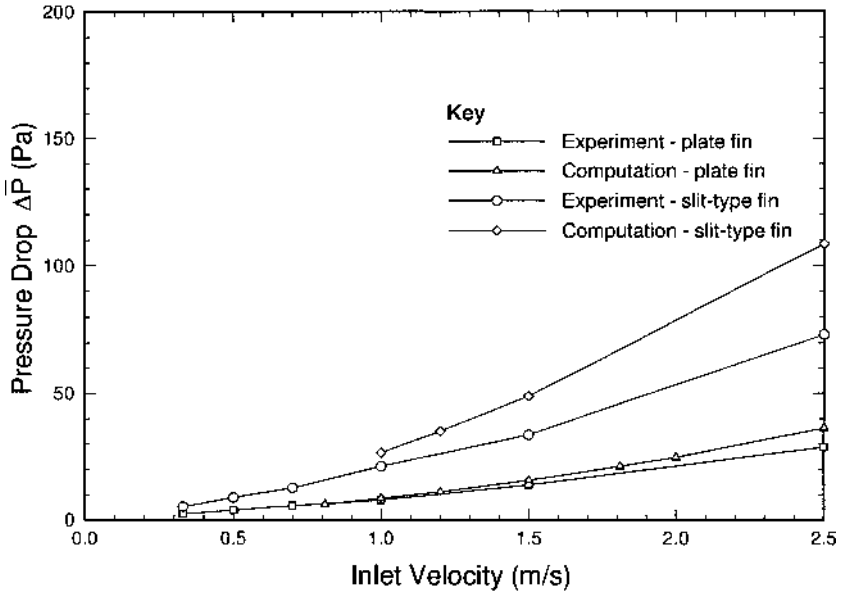

Figure 4.
A comparison study of computed and measured pressure drops against inlet velocities summarized in Table I

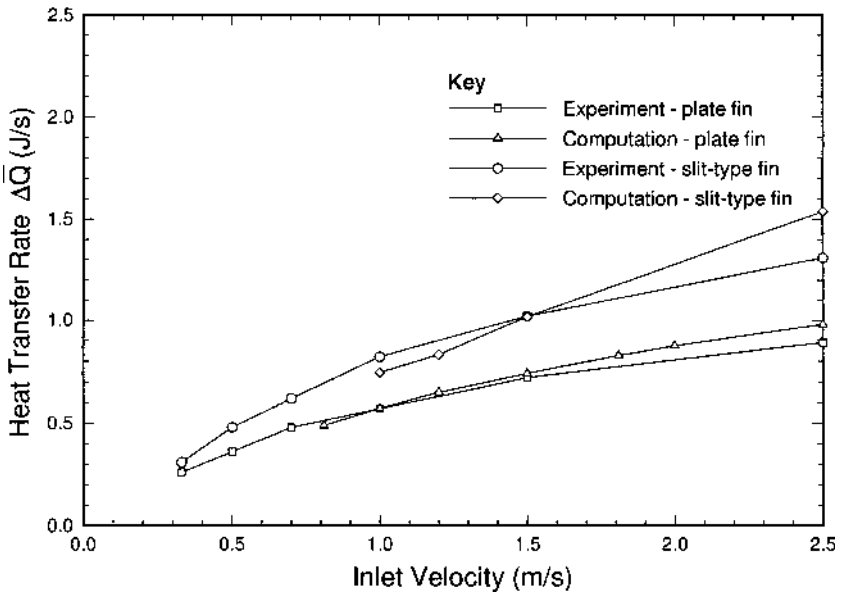

Figure 5.
A comparison study of computed and measured heat transfer rates against inlet velocities summarized in Table I

surfaces or in the horseshoe vortex. Another factor causing the local heat transfer enhancement is the high temperature on the fin surface and low bulk temperature. We also plot in Figure 8 the heat flux distribution on the fin configured in Figure 2. A trend similar to that for the plate fin is observed in that $\dot{q}$ takes on larger values in regions upstream of the tube.

With the computed local values of $\dot{q}$ on the fin surface, it was easy for us to compute some span-averaged quantities of physical significance to illuminate

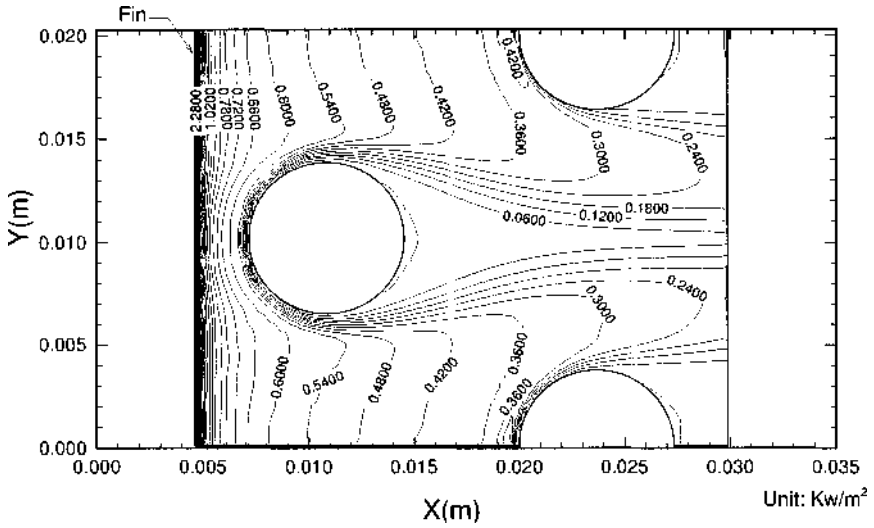

Figure 6.
A contour plot of heat flux $\dot{q}$ on the plate fin for the case of Re = 124 (or inlet velocity is 1.2m/s)

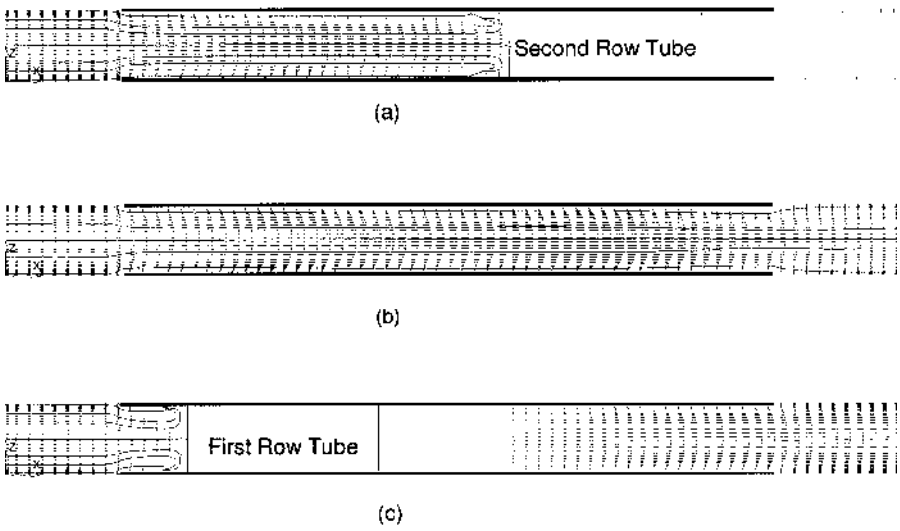

Figure 7.
Velocity vector plots and particle tracers: (a) at $y = 0$ plane; (b) at $y = \frac{B}{4}$ plane; (c) at $y = \frac{B}{2}$ plane

the heat transfer ability. Figure 9 shows the span-averaged Nusselt number in the streamwise direction for the plate fin under running inlet conditions given in Table I. Clearly revealed by this figure is an abrupt increase of *Nu* ahead of the tube. As noted earlier, this increase is the result of the horseshoe vortex formation. Also revealed is a gradual drop of *Nu* from its maximum value at the leading edge due to the boundary layer development. For the sake of completeness, we also plot the span-averaged $\dot{q}_{sp}$ in Figure 10 for the slit-type finned-tube exchanger.

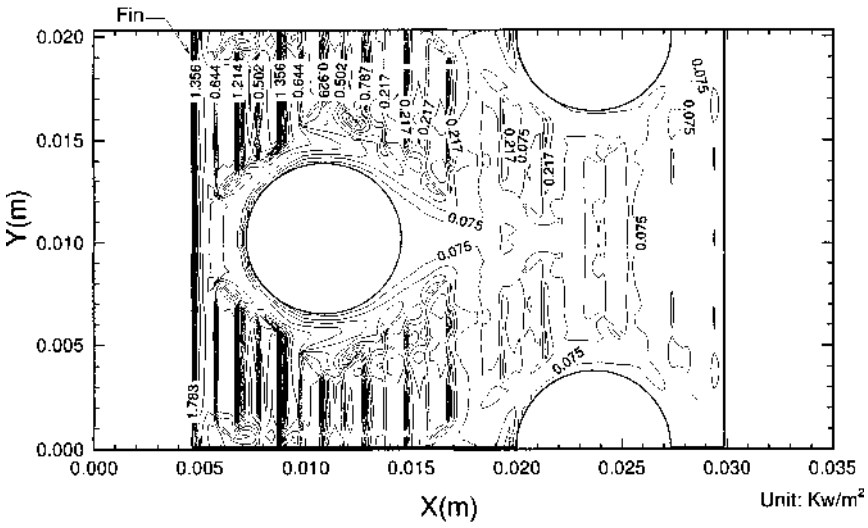

Figure 8.
Contour of heat fluxes on the $z = 0$ surface of slit-type heat exchanger

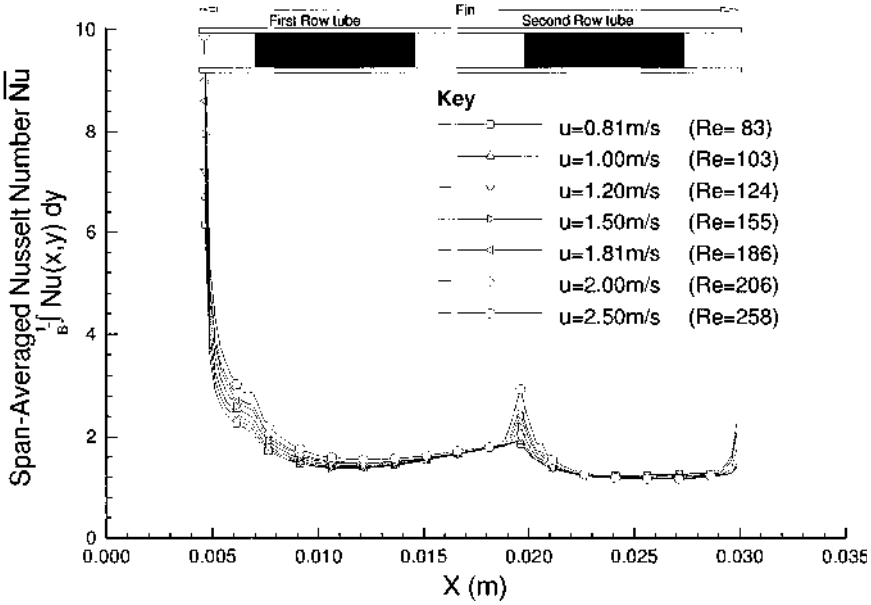

Figure 9.
Span-averaged Nusselt numbers in the streamwise direction as a function of Reynolds numbers for the plate fin under investigation

Flow physics in the passage

Another quantity that is crucial to heat transfer design is the pressure drop, as shown in Figure 11 for two investigated fins, in the flow passage. Figure 11 plots the span-averaged pressures for two types of investigated fins. The drop

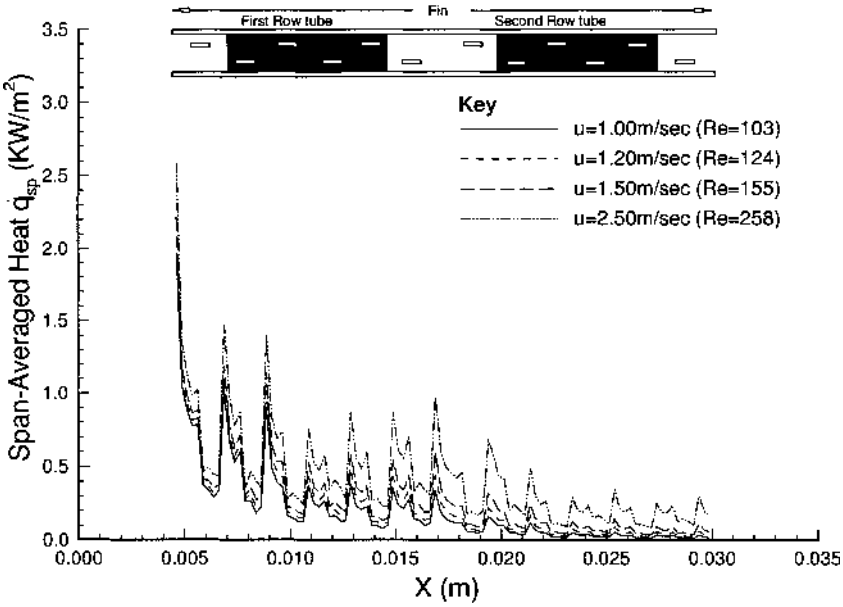

Figure 10.
Span-averaged q_{sp} in the streamwise direction as a function of Reynolds numbers for the slit-type fin under investigation

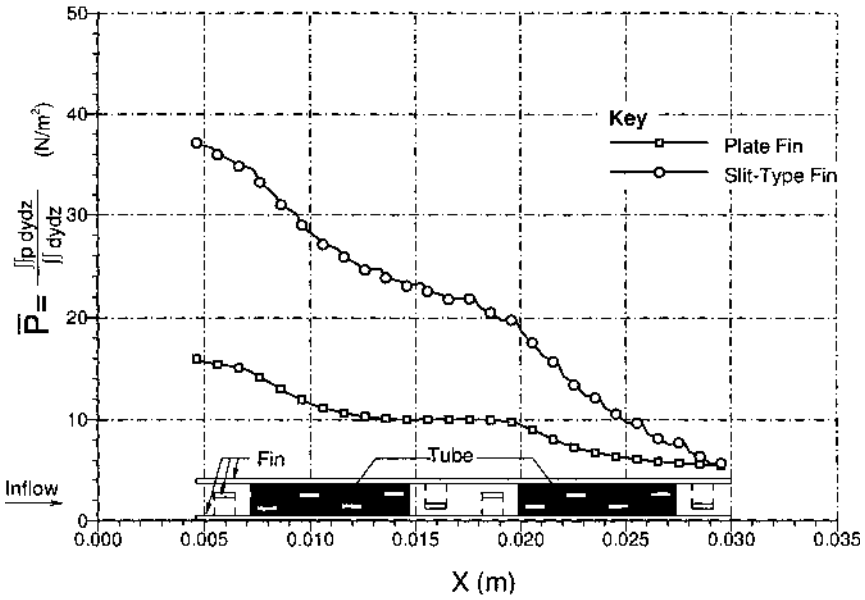

Figure 11.
Averaged pressure distribution in the streamwise direction for plate and slit-type fins

in the pressure is mainly due to the established tube form-drag. A comparatively mild pressure drop is found in front of and behind the tube.

We now address the fluid dynamic aspect. Since the physical domain under investigation was bounded by two fairly narrow fins in which circular tubes were staggered, the flow structure was definitely three-dimensional. This is in strong contrast to the cross flows in regions around infinite length cylinders. Furthermore, perforation of the fin plate caused termination of the developing boundary layer. This, together with the stagnant nature of the flow in regions adjacent to the perforated fin surface, caused a prevailing secondary flow in the transverse plane. For better representation of the three-dimensional nature of the flow, we released marker particles in appropriate locations to track their journey. As Figure 12 shows, particles are entrained by the longitudinal vortices which are generated by the perforated fin. The formation of longitudinal vortices is due mainly to the pressure difference between the pressure and the suction sides of the perforated fin. It is this local formation of longitudinal vortices that causes the spanwise particle motion. With this spanwise mixing mechanism, increased heat transfer is expected. The evidence showing a better heat transfer over that without fin perforation is plotted in Figure 13.

The reason for the heat transfer enhancement is the spiraling nature of the horseshoe vortex formed in front of the tube. The center of the horseshoe vortex, as seen in Figure 14, is regarded as a critical point. By definition, particles adjacent to the rotation center of the horseshoe vortex spiral toward this point. This aids the mixing of the fluid flow and, thus, the heat transfer. A

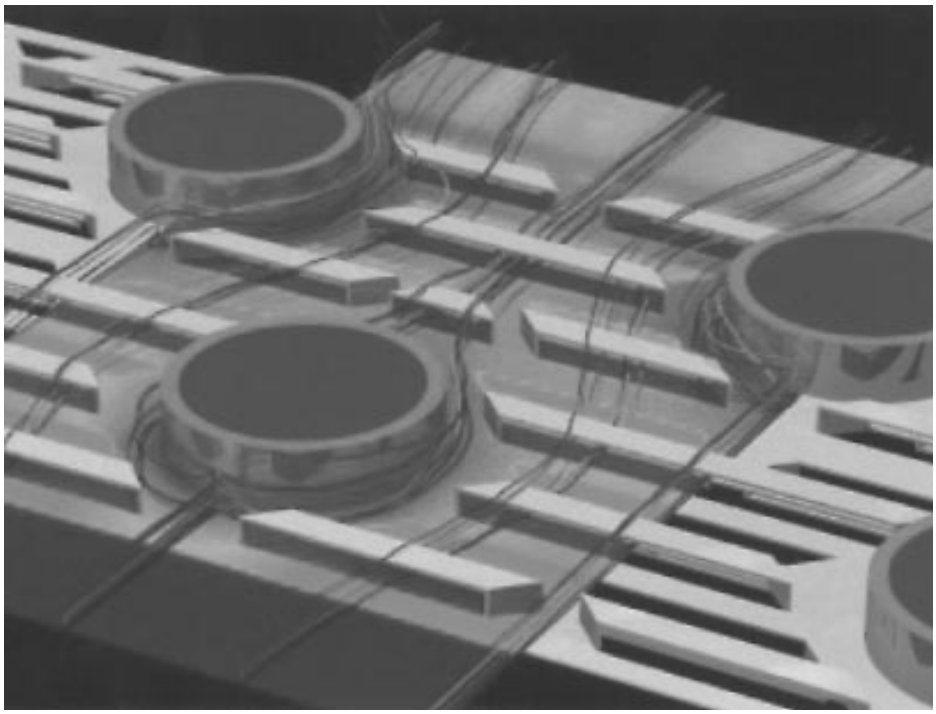

Figure 12.
Particle trajectories in the flow passage between two slit fins

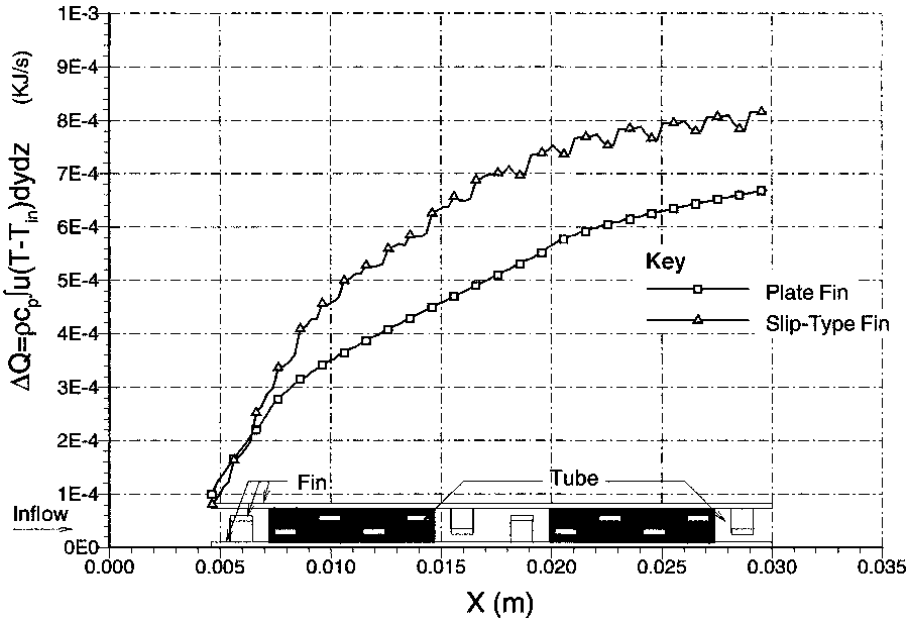

Figure 13.
Span-averaged heat transfer in the streamwise direction for two investigated fin surfaces

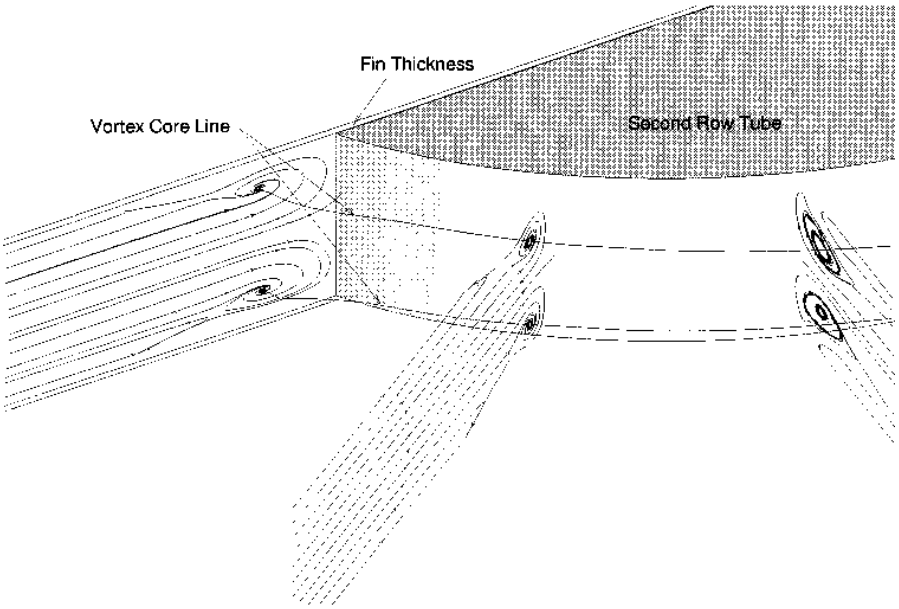

Figure 14.
An illustration of vortical core line in front of the second-row of the cylinder

collection of these horseshoe vortex centers forms a vortical core line. Particles near this line are entrained towards the vortex center and proceed downstream in a spiraling nature. This implies that the mixing of fluid flows is essentially a three-dimensional phenomenon.

Conclusions

This paper has presented an assessment study for evaluating the effectiveness of two investigated types of fins in enhancing heat transfer. The numerical method employed here to explore the flow complexities has been verified analytically as well as experimentally. This study has explored in depth the three-dimensional nature of the flow, which explains why fins with perforations have advantages over plate fins used in the conjugate heat exchanger. For a better understanding of the flow physics, we have depicted the horseshoe vortex through the computed solutions.

References

Abdallah, S. (1987), "Numerical solution for the incompressible Navier-Stokes equations in primitive variables using a non-staggered grid, II.", *J. Comp. Phys.*, Vol. 70, pp. 193-202.

Fiebig, M., Chen, Y., Grosse-Gorgemann, A. and Mitra, N.K. (1995b), "Conjugate heat transfer of a finned tube Part B: heat transfer augmentation and avoidance of heat transfer reversal by longitudinal vortex generators", *Numerical Heat Transfer,* Part A, Vol. 28, pp. 147-55.

Fiebig, M., Grosse-Gorgemann, A., Chen, Y. and Mitra, N.K. (1995a), "Conjugate heat transfer of a finned tube Part A: heat transfer behavior and occurrence of heat transfer reversal", *Numerical Heat Transfer,* Part A, Vol. 28, pp. 133-46.

Ladyzhenskaya, O.A. (1963), *Mathematical Problems in the Dynamics of a Viscous Incompressible Flow,* Gordon and Breach, New York, NY.

Leonard, B.P. (1979), "A stable and accurate convective modelling procedure based on quadratic upstream interpolation", *Comput. Methods Appl. Mech. Eng.,* Vol. 19, pp. 59-98.

Patankar, S.V. (1980), *Numerical Heat Transfer and Fluid Flow,* Hemisphere, Washington, DC.

Saboya, F.E.M. and Sparrow, E.M. (1974), "Effect of tube relocation on the transfer capabilities of fin and tube heat exchanger", *J. of Heat Transfer, Transactions of the ASME*, Vol. 96 No. 3, pp. 421-3.

Saboya, E E.M. and Sparrow, E.M. (1976), "Transfer characteristics of two-row plate fin and tube heat exchanger configurations", *Int. J. of Heat and Mass Transfer,* Vol. 19, pp. 41-9.

Sheu, W.H. and Lee, S.M. (1996), "A segregated solution algorithm for incompressible flows in general coordinates", *Int. J. Numer. Methods Fluids,* Vol. 22, pp. 1-34.